Chinese Chemical Letters 33 (2022) 298–303

Contents lists available at ScienceDirect

Chinese Chemical Letters

journal homepage: www.elsevier.com/locate/cclet

Orange-emitting bimetallic nanoclusters combined with cyan-emitting Fe@TAOH as white light-emitting materials

Wenying Mi, Na Shao*

College of Chemistry, Beijing Normal University, Beijing 100875, China

ARTICLE INFO

Article history:
Received 6 March 2021
Revised 6 April 2021
Accepted 14 June 2021
Available online 25 June 2021

Keywords:
Metal nanoclusters
Salt-mediated precipitation
Fe@TAOH MOFs
Self-assembly
White light-emitting materials

ABSTRACT

White-light-emitting diodes (WLEDs) possess many merits, such as high efficiency and stability. Developing cost-effective, environmentally friendly, high-performance luminophores to achieve high-quality, full-spectrum, white lighting is of great importance to the construction and progress of WLEDs. In this work, solid-state, highly luminescent orange-emitting nanoclusters ($MgCl_2$-Lys-Ag/Au NCs) were prepared *via* the salt-induced precipitation of Lys-Ag/Au NCs from solution, which showed a high absolute quantum yield of 44.5%. A cyan-emitting metal-organic framework (MOF)-like nanomaterial (named Fe@TAOH) was also prepared by the self-assembly of the coordination compound of Fe^{3+} and TAOH acted upon by H_3PO_4 *via* H-bonding and π-π stacking interactions, which showed an emission peak at 485 nm and an absolute quantum yield of 21.7%. The potential application of the two facile-synthesis, low toxicity, and highly luminescent materials in WLEDs was investigated. The WLEDs was constructed by coating powdered Fe@TAOH and $MgCl_2$-Lys-Ag/Au NCs samples on commercial GaN LED chip with 365 nm emissions, and it exhibited acceptable white light characteristics with a CIE color coordinates and a color rendering index (CRI) of (0.28, 0.34) and 79.6, respectively, implying good prospects in the field of WLEDs.

White-light-emitting diodes (WLEDs) have attracted attention in solid-state lighting due to their advantages of a high luminous efficiency, long lifetime, high energy conversion, and fast response time [1,2]. Most commercial WLEDs fabricated by coating yellow-emitting phosphors onto blue-emitting LED chips suffer from a low color rendering index (CRI) and highly correlated color temperature due to the absence of a red-emitting component [3,4]. The strong blue light produced by the blue chips is also harmful to human health. Near-ultraviolet LED chips mixed with tricolor phosphors (blue, green, and red) are candidates for fabricating WLEDs [5,6]. Nevertheless, an obvious spectra gap in the cyan region (480–520 nm) was locked out for this kind of WLED, thus restricting their potential application in high-quality lighting [7]. WLEDs with higher performance, such as an enhanced CRI, can be obtained by introducing cyan-emitting phosphors into tricolor phosphors or red-emitting phosphors to fill the cyan gap [8,9].

In addition, most commercial WLEDs rely on the up-conversion of luminescent materials doped with rare earth elements, which suffers from several issues such as high cost, limited resources, and complex synthetic procedures [10–12]. Although much attention has been paid to semiconductor quantum dots in the field of white-light phosphors fields due to their high fluorescence quantum yield [13,14], the toxicity of the heavy metal component restricts their wider application. It is of importance to explore simple synthesis, low-cost, and environmentally friendly luminous materials for the fabrication of white-light phosphors.

Metal nanoclusters (MNCs) have attracted a great deal of interest in the field of WLEDs in recent years [15–17], due to their strong luminescence, high photostability, tunable luminance, and especially facile synthesis and low toxicity [18–21]. To date, most nanocluster-based phosphors have taken advantage of the aggregation-induced emission (AIE) property to acquire stronger luminescence in solid state; the commonly utilized method to prepare solid MNCs is by drying solvent directly, which suffers from being time-consuming and difficult for mass production. Thus, it is still of great significance to prepare highly luminescent solid-state MNCs by simple methods. Herein, highly luminescent solid-state MNCs were prepared *via* the salt-mediated precipitation of MNCs from solution. The prepared solid $MgCl_2$-Lys-Ag/Au NCs with orange emission exhibited an enhanced fluorescence quantum yield compared with the solid Lys-Ag/Au NCs (from 34.5% to 44.5%).

Terephthalic acid (TA) and its derivatives are commonly used for synthesizing iron-based metal-organic frameworks (Fe-MOFs) [22,23], where TA is oxidized to TAOH in the presence of hydroxyl radical, showing strong fluorescence [24,25]. Here, a cyan-emitting

* Corresponding author.
E-mail address: shaona@bnu.edu.cn (N. Shao).

https://doi.org/10.1016/j.cclet.2021.06.039
1001-8417/

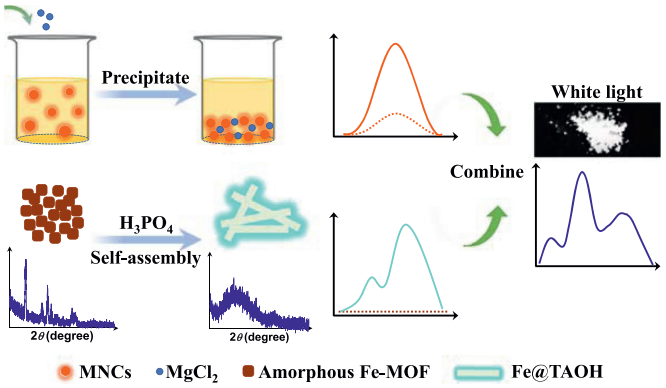

Scheme 1. Schematic of the preparation of orange-emitting $MgCl_2$-Lys-Ag-/Au NCs and cyan-emitting Fe@TAOH, and their combination for white light materials.

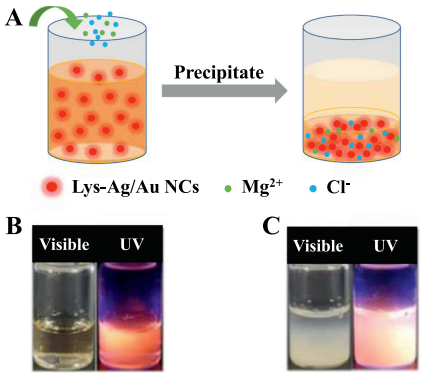

Fig. 2. (A) The process of preparing $MgCl_2$-Lys-Ag/Au NCs. Photographs of Lys-Ag/Au NCs in the absence (B) and presence (C) of $MgCl_2$ solution under visible and UV light.

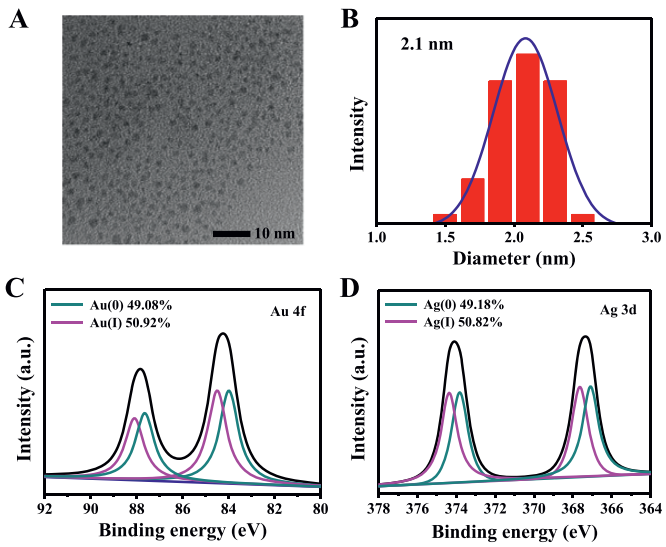

Fig. 1. (A) TEM image and (B) size distribution of Lys-Ag/Au NCs. XPS spectra exhibiting the binding energy of Au element (C) and Ag element (D) in the Lys-Ag/Au NCs.

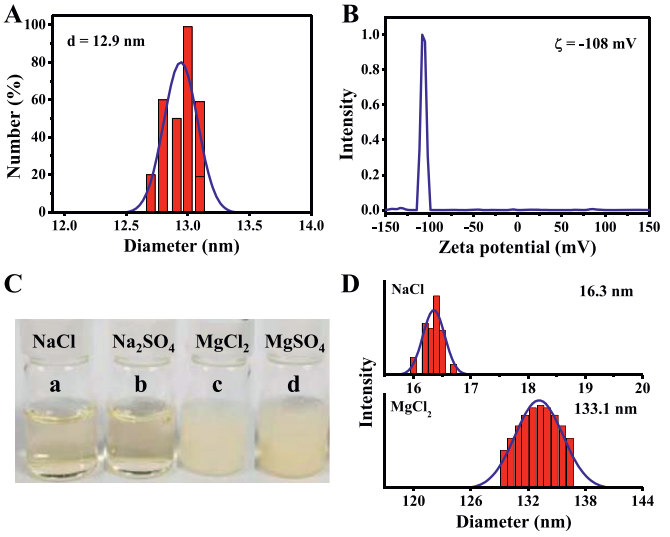

Fig. 3. (A) Dynamic light scattering (DLS) analysis and (B) Zeta potential measurements of the Lys-Ag/Au NCs. (C) Photographs of the Lys-Ag/Au NCs added with different salt solution and (D) corresponding DLS measurements. The concentration of NaCl was 200 mmol/L, and that of Na_2SO_4, $MgCl_2$ and $MgSO_4$ were 100 mmol/L.

nanomaterial (named Fe@TAOH) prepared by the self-assembly of the complex of Fe^{3+} and 2-hydroxy terephthalic acid (TAOH) *via* the reaction of TA and Fenton reagent acted upon by phosphoric acid was developed. The prepared Fe@TAOH showed a maximum emission peak at 485 nm with an absolute fluorescence quantum yield of 21.7%.

The WLEDs fabricated by encapsulating orange-emitting $MgCl_2$-Lys-Ag/Au NCs and cyan-emitting Fe@TAOH powders on a commercially available 365 nm GaN LED chip showed a CIE color coordinates of (0.28, 0.34) and a CRI of 79.6, demonstrating their feasibility in WLED applications. The synthesis of the solid $MgCl_2$-Lys-Ag/Au NCs and Fe@TAOH was environmentally friendly and cost-effective. The preparation of the two luminescent materials, as well as their combination for white-light materials, is shown in Scheme 1.

Transmission electron microscopy (TEM) was employed to characterize the morphology of the as-prepared Lys-Ag/Au NCs (Fig. 1A), which showed high dispersity with an average diameter of 2.1 nm (Fig. 1B). X-ray photoelectron spectroscopy (XPS) was also performed to prove the existence of Au and Ag elements in Lys-Ag/Au NCs (Figs. 1C and D). Inductively coupled plasma atomic emission spectroscopy analysis confirmed that the ratio of Au to Ag in the Lys-Ag/Au NCs was 5.02 (Table S1 in Supporting information), which was consistent with that of Au^{3+} to Ag^{+} in the precursor solution for synthesizing the Lys-Ag/Au NCs.

It is known that protein will precipitate out of solution in the presence of high concentrations of salt, referred to as protein salting-out [26,27]. Therefore, it was speculated that protein-capped nanoclusters would precipitate out of the solution when salt solution was introduced, which could supply a novel method to prepare solid-state luminescent nanoclusters. As Fig. 2A shows, when the $MgCl_2$ solution was added into the as-prepared Lys-Ag/Au NCs, the clear solution (Fig. 2B) became cloudy immediately and a large amount of white precipitate (Fig. 2C) formed (denoted as $MgCl_2$-Lys-Ag/Au NCs), which showed intense orange-emission under UV lamp excitation.

To investigate the Lys-Ag/Au NCs precipitation induced by $MgCl_2$ solution, first, dynamic light scattering experiments were carried out to determine the hydrodynamic diameter and surface charge of the Lys-Ag/Au NCs. As shown in Figs. 3A and B, the diameter of the MNCs was 12.9 nm, and the Zeta potential was about −108 mV, indicating that the Lys-Ag/Au NCs dispersed well in the solution and possessed a negative surface charge. As shown in Fig. 3C, the Lys-Ag/Au NCs solution became cloudy after $MgCl_2$ and $MgSO_4$ were added, while those with added NaCl or Na_2SO_4 were still clear. As shown in Fig. 3D, the hydrodynamic diameter of

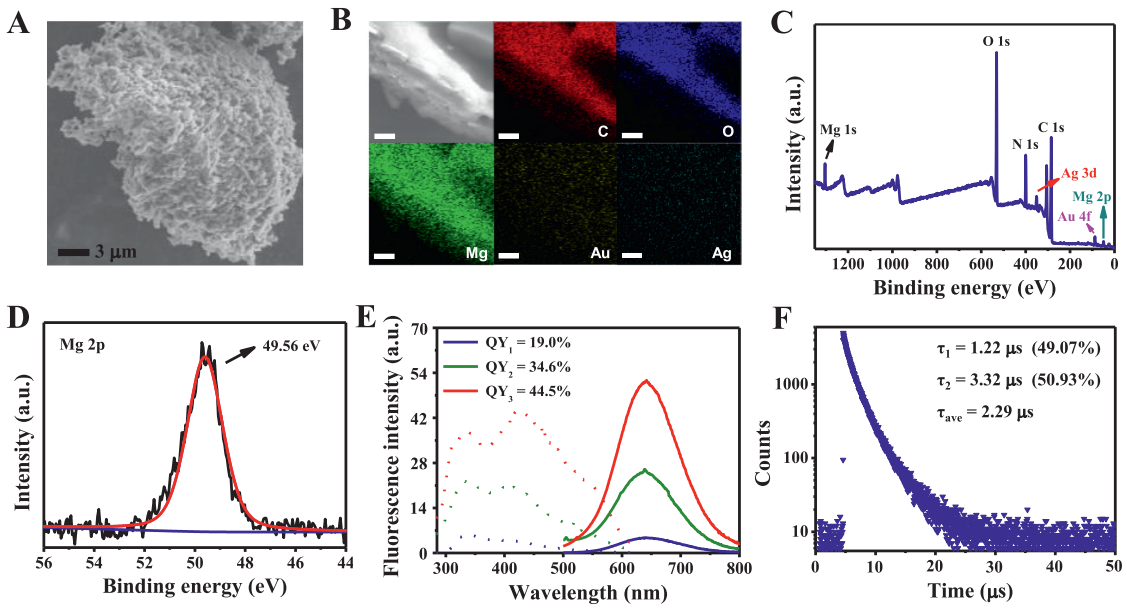

Fig. 4. (A) SEM image and (B) elemental mapping analyses (the scale bar is 2 μm) of $MgCl_2$-Lys-Ag/Au NCs. (C) Survey XPS spectra of $MgCl_2$-Lys-Ag/Au NCs. (D) XPS spectrum exhibiting the binding energy of Mg element in the $MgCl_2$-Lys-Ag/Au NCs. (E) Fluorescence excitation and emission spectra of the Lys-Ag/Au NCs in solution (blue line) and in solid (green line) as well as that of the solid $MgCl_2$-Lys-Ag/Au NCs (red line) (QY presented the absolute quantum yield). (F) Time-resolved fluorescence lifetime analysis of the $MgCl_2$-Lys-Ag/Au NCs. For interpretation of the references to color in this figure legend, the reader is referred to the web version of this article.

the Lys-Ag/Au NCs increased to 133.1 nm after $MgCl_2$ was added, while it showed little change when NaCl was added.

The effect of salt ions on MNC precipitation was further explored. As shown in Fig. S1A (Supporting information), precipitate could form even when 50 mmol/L of $MgSO_4$ was added into the Lys-Ag/Au NCs solution, and the precipitate increased with the increasing salt concentration. However, for the MNCs with added Na_2SO_4 (Fig. S1B in Supporting information), no precipitate was generated, even when the salt concentration was increased to 1 mol/L. The results demonstrated that cation-like Mg^{2+} can connect with the Lys-Ag/Au NCs *via* coordination interactions except for electrostatic interactions. These interactions between the cation and the MNCs were also proved by the fact that $(NH_4)_2SO_4$ could make the Lys-Ag/Au NCs precipitate but Na_2SO_4 with the same concentration could not (Fig. S2 in Supporting information). NH_4^+ with the negatively charged Lys-Ag/Au NCs, not only *via* electrostatics, but also intermolecular hydrogen bonding. It was speculated that the surface charge of the Lys-Ag/Au NCs was shielded by the ions with the opposite charge, thus leading to the precipitation of Lys-Ag/Au NCs due to the reduced electrostatic repulsion force among the MNCs.

Subsequently, the composition and morphology of the prepared $MgCl_2$-Lys-Ag/Au NCs were studied. The $MgCl_2$-Lys-Ag/Au NCs showed a net-work structure (Fig. 4A) composed of C, N, O, Au, Ag, and Mg elements, as confirmed by SEM elemental mapping analysis (Fig. 4B) and XPS measurements (Fig. 4C). The low signal for Au and Ag elements in the SEM elemental mapping may be attributed to Au and Ag being embedded by surface ligands [28]. XPS measurements (Fig. 4D) also indicated the existence of Mg^{2+}, which most likely connects to the Lys-Ag/Au NCs by linking with the carboxyl group of the ligands *via* electrostatic and coordination interactions. The cross-linked morphology of the Lys-Ag/Au NCs with added $MgCl_2$ solution was further supported by TEM measurements (Fig. S3 in Supporting information).

Fluorescence spectra were measured to investigate the optical properties of the $MgCl_2$-Lys-Ag/Au NCs. As shown in Fig. 4E, the fluorescence intensity of the solid $MgCl_2$-Lys-Ag/Au NCs at the maximum emission wavelength was remarkably enhanced compared with that of the Lys-Ag/Au NCs in solution and as a solid, increasing the absolute quantum yield to 44.5% from 19.0% to 34.6%, respectively. The fluorescence enhancement of the solid $MgCl_2$-Lys-Ag/Au NCs can be attributed to the restriction of nonradiative motions of the surface ligands and an enhanced ligand-to-metal charge transfer by forming a cross-linked network connected by Mg^{2+} [29,30]. The fluorescence decay curve of the $MgCl_2$-Lys-Ag/Au NCs presented in Fig. 4F shows that the average lifetime of the $MgCl_2$-Lys-Ag/Au NCs was 2.29 μs after combining the two components, each with lifetimes of 1.22 μs (49.07%) and 3.32 μs (50.93%), respectively.

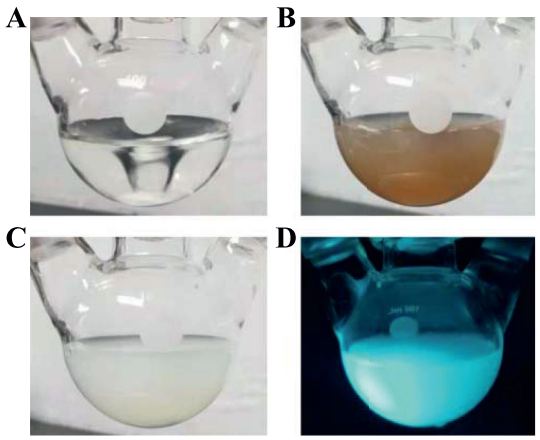

Fig. 5. The photographs of (A) TA dissolved in alkali solution, (B) Fenton reagent added into (A), (C) the component in (B) added with phosphoric acid, and (D) the prepared Fe@TAOH under UV light. For interpretation of the references to color in this figure, the reader is referred to the web version of this article.

The cyan-emitting Fe@TAOH was then prepared. A nonluminous, brick-red precipitate (named Fe-TAOH) was generated when H_2O_2 was added into the mixture solution of TA and Fe^{2+} (Fig. 5A and B), and then white precipitate formed when phosphoric acid (H_3PO_4) was introduced into the above brick-red precipitate

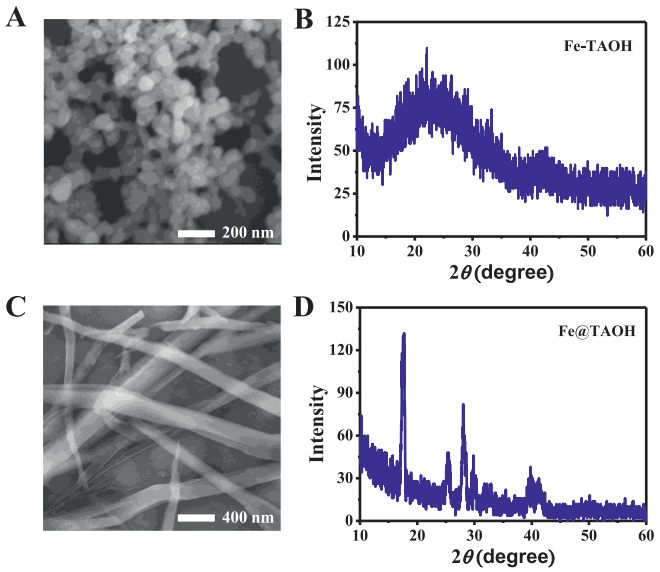

Fig. 6. (A) SEM image and (B) XRD analysis of the Fe-TAOH. (C) SEM image and (D) XRD analysis of Fe@TAOH. (For interpretation of the references to color in this figure, the reader is referred to the web version of this article.)

(Fig. 5C). The obtained white precipitate (denoted as Fe@TAOH) emitted strong cyan fluorescence under the UV lamp (Fig. 5D).

The chemical composition of Fe@TAOH was examined. As displayed by X-ray photoelectron spectroscopy (XPS) measurements shown in Fig. S4A (Supporting information), Fe@TAOH was composed of C, O, and Fe elements, where Fe element came from the Fenton reagent. Fe $2p_{1/2}$ and Fe $2p_{3/2}$ peaks were located at 726.4 and 712.9 eV (Fig. S4B) (Supporting information)), which implied that the valence state of the Fe element in Fe@TAOH was +3 and verified the production of Fe^{3+} from the Fenton reaction. Electrospray ionization mass spectrometry (ESI-MS) was also employed to determine the chemical structure of Fe@TAOH, as shown in Fig. S5 (Supporting information). The mass peak at 338.3433 corresponded to the composition of $Fe_{2.5}(TAOH)(H_2O)$, and the mass peak at 675.6778 was a diploid peak corresponding to composition of $Fe_5(TAOH)_2(H_2O)_2$.

SEM imaging showed that the brick-red precipitate was composed of spherical particles with a uniform size, as shown in Fig. 6A. The XRD pattern showed a bulging peak shape (Fig. 6B), implying the brick precipitate had an amorphous morphology [31]. The white precipitate (Fe@TAOH) showed a regular bar structure in the SEM experiments (Fig. 6C). The XRD pattern of Fe@TAOH shown in Fig. 6D displayed several distinct, sharp peaks, implying Fe@TAOH had a crystalline structure [31]. It is speculated that the amorphous Fe-MOF self-assembled to form a regular bar structure under the influence of hydrogen bonding and π-π interaction in the presence of H_3PO_4 [32]. The FT-IR spectra of TA, Fe-TAOH, and Fe@TAOH are shown in Fig. 7A. Compared with that of TA, the characteristic absorption peak of hydroxy (O–H) bonds at 3424 cm^{-1} demonstrated that TA was oxidized to TAOH by the Fenton reagent. The disappearance of the –COOH peak at 2500–3300 cm^{-1} and appearance of C=O peaks from the $–COO^-$ group at 1556 cm^{-1} and 1389 cm^{-1} showed that TAOH coordinated with iron, for that carboxyl group can coordinate with Fe^{3+} [33,34]. The absorption peak of the C–H bonds in phenyl at 756 cm^{-1} and that of Fe–O bonds at 535.43 cm^{-1} further indicated the formation of TAOH and its combination with Fe.

The results indicated that the luminescent white precipitate of Fe@TAOH can be generated *via* TA reacting with the products (Fe^{3+} and $^{\bullet}OH$) of the Fenton reagent. Non-fluorescent TA was oxidized to fluorescent hydroxy terephthalic acid (TAOH) by $^{\bullet}OH$ from the Fenton reaction. The brick-red precipitate of Fe-TAOH formed by the coordination of TAOH with Fe^{3+} was nonluminous due to the quenching effect of Fe^{3+} on TAOH However, by adding H_3PO_4 to the brick-red precipitate, the nonluminous Fe-TAOH proceeded to self-assemble to form luminous Fe@TAOH.

The optical properties of the Fe@TAOH were investigated. As Fig. 7B shows, the Fe@TAOH had wide excitation spectra ranging from 255 to 465 nm, with two distinct peaks located at 318 and 420 nm. Fe@TAOH showed two emission peaks located at 396 and 485 nm when excited at 318 nm; when excited at 420 nm, only one emission peak located at 490 nm appeared, and with an absolute quantum yield of 21.7%. The time-resolved fluorescence lifetime of Fe@TAOH was also determined, as shown in Fig. 7C. The average lifetime of Fe@TAOH was 6.49 ns after combining the two components, each with lifetimes of 3.93 ns (21.98%) and 7.21 ns (78.02%).

The fluorescence emission spectra of the cyan-emitting Fe@TAOH ranged from 325 to 650 nm (Fig. 8A), while that of the orange-emitting $MgCl_2$-Lys-Ag/Au NCs ranged from 455 to 800 nm (Fig. 8B). The emission of the two components can almost cover the whole visible spectral range from 400 to 800 nm, which is beneficial to the fabrication of white-light-emitting materials. Meanwhile, the excitation spectra of Fe@TAOH and $MgCl_2$-Lys-Ag/Au NCs overlapped well from 290 to 465 nm, ensuring that both components of the mixture can be excited under a certain excitation light source.

To investigate the feasibility of the prepared $MgCl_2$-Lys-Ag/Au NCs and Fe@TAOH in the application of white-light-emitting materials, their photostability against storage time was first investigated. As shown in Fig. S6 (Supporting information), the fluorescence intensity of Fe@TAOH and $MgCl_2$-Lys-Ag/Au NCs displayed minor changes after three months of storage in a refrigerator at 4 °C under dark conditions. In addition, the obtained Fe@TAOH and $MgCl_2$-Lys-Ag/Au NCs solids were insoluble in water (Fig. S7

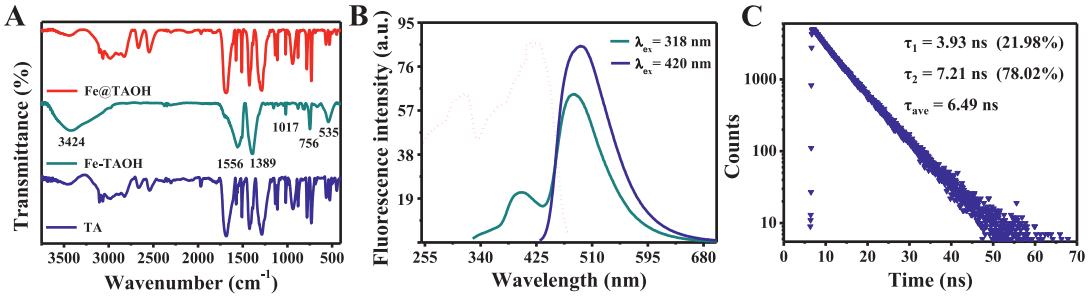

Fig. 7. (A) FT-IR spectra of the TA (blue line), Fe-TAOH (green line) and Fe@TAOH (red line). (B) Fluorescence excitation and emission spectra of solid Fe@TAOH. (C) Time-resolved fluorescence lifetime analysis of Fe@TAOH. (For interpretation of the references to color in this figure legend, the reader is referred to the web version of this article.)

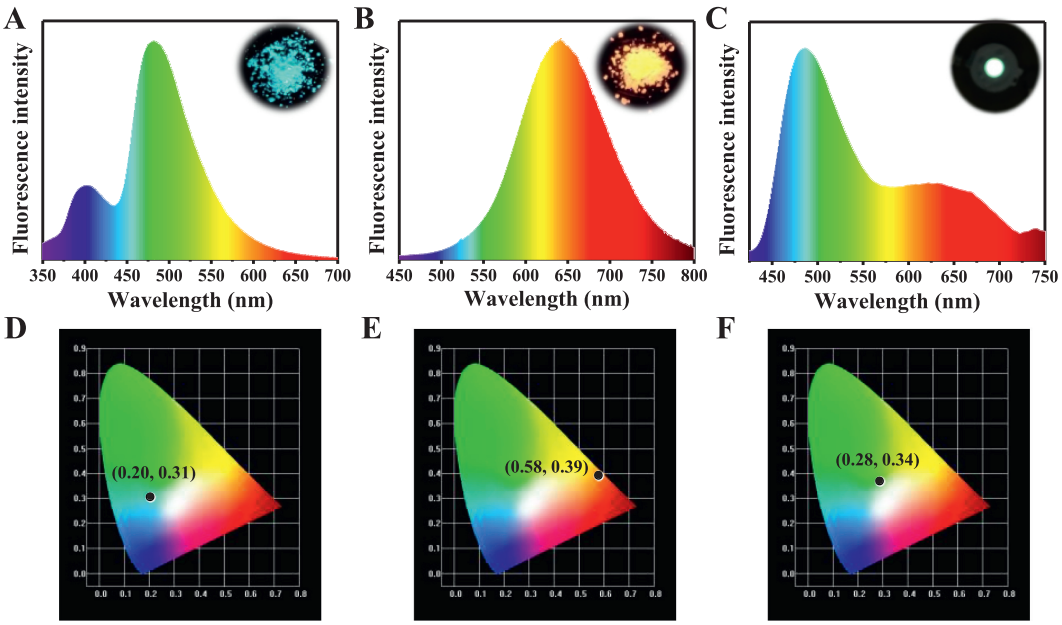

Fig. 8. Emission spectra of (A) Fe@TAOH, (B) $MgCl_2$-Lys-Ag/Au NCs and (C) WLEDs fabricated by Fe@TAOH and $MgCl_2$-Lys-Ag/Au NCs (the insets were the photographs of corresponding materials under UV lamp and WLEDs). And CIE color coordinates of cyan-emitting Fe@TAOH (D), orange-emitting $MgCl_2$-Lys-Ag/Au NCs (E) and WLEDs (F). For interpretation of the references to color in this figure legend, the reader is referred to the web version of this article.

in Supporting information), implying they were stable in high-moisture circumstances. Importantly, the Fe@TAOH and $MgCl_2$-Lys-Ag/Au NCs showed excellent photostability against long exposures to light irradiation (Fig. S8 in Supporting information), which is beneficial for luminescent material applications.

Due to their distinctly advantageous properties, Fe@TAOH and $MgCl_2$-Lys-Ag/Au NCs were utilized to fabricate WLEDs. The cyan-emitting Fe@TAOH and orange-emitting $MgCl_2$-Lys-Ag/Au NCs have color coordinates of (0.20, 0.31) (Fig. 8D) and (0.58, 0.39) (Fig. 8E), respectively. The WLEDs fabricated by coating Fe@TAOH and $MgCl_2$-Lys-Ag/Au NCs powders on a commercial UV-light (365 nm) LED chip showed an emission spectra ranging from 425 to 800 nm (Fig. 8C), and emitted white light under the excitation of UV-light chip (the inset of Fig. 8F). As shown in Table S2 (Supporting information), the performance of WLEDs was measured and it displayed an acceptable white light emission with CIE color coordinates of (0.28, 0.34), and showed high CRI of 79.6 and correlated color temperature (CCT) of 5299. These results demonstrated that our prepared Fe@TAOH and $MgCl_2$-Lys-Ag/Au NCs have prospects in the application of WLEDs.

In summary, orange-emitting $MgCl_2$-Lys-Ag/Au NCs and cyan-emitting Fe@TAOH were prepared and employed to fabricate WLEDs. Highly luminescent solid-state $MgCl_2$-Lys-Ag/Au NCs were prepared *via* a convenient method involving the salt-induced precipitation of Lys-Ag/Au NCs out of the parent solution, which exhibited a high absolute quantum yield (44.5%), large Stokes shift (215 nm), and good photostability. In addition, cyan-emitting phosphors prepared *via* the reaction of TA and Fenton reagent under the guidance of phosphoric acid were developed. The prepared Fe@TAOH had a maximum emission wavelength at 485 nm, with wide excitation spectra ranging from 255 to 465 nm, as well as an absolute quantum yield of 21.7%. The excitation spectra of the Fe@TAOH and $MgCl_2$-Lys-Ag/Au NCs overlapped well from 290 to 465 nm, and the emission of the two components combined covered the whole visible spectral range from 400 to 800 nm, which showed an acceptable white emission with CIE color coordinates of (0.28, 0.34) and high CRI of 79.6. This work provides a simple method to quickly prepare highly efficient, environmentally friendly, and low-cost emitting phosphors for solid-state luminescence. The prepared nanomaterials have bright prospects for applications in the field of WLEDs.

Declaration of competing interest

The authors declare that they have no known competing financial interests or personal relationships that could have appeared to influence the work reported in this paper.

Acknowledgment

The project was supported by the National Natural Science Foundation of China (No. 22074007).

Supplementary materials

Supplementary material associated with this article can be found, in the online version, at doi:10.1016/j.cclet.2021.06.039.

References

[1] V. Fernández-Luna, P.B. Coto, R.D. Costa, Angew. Chem. Int. Ed. 57 (2018) 8826–8836.
[2] J. Cho, J.H. Park, J.K. Kim, E.F. Schubert, Laser Photonics Rev. 11 (2017) 1600147.
[3] H. Ji, L. Wang, Y. Cho, et al., J. Mater. Chem. C 4 (2016) 9872–9878.
[4] X. Huang, H. Guo, L. Sun, T. Sakthivel, Y. Wu, J. Alloy. Compd. 787 (2019) 865–871.
[5] S. Wu, P. Xiong, X. Liu, et al., J. Mater. Chem. C 8 (2020) 16584–16592.
[6] Z. Wang, Q. Meng, C. Wang, D. Fan, Y. Wang, J. Mater. Chem. C 8 (2020) 14548–14558.
[7] J. Liang, B. Devakumar, L. Sun, et al., J. Mater. Chem. C 8 (2020) 4934–4943.
[8] D. Liu, X. Yun, G. Li, et al., Adv. Opt. Mater. 8 (2020) 2001037.
[9] L. Sun, B. Devakumar, J. Liang, et al., J. Mater. Chem. C 8 (2020) 1095–1103.
[10] R.S. Yadav, S.B.Rai Monika, S.J. Dhoble, Prog. Solid State Chem. 57 (2020) 100267.
[11] H. Zhang, H. Zhang, A. Pan, et al., Adv. Mater. Technol. 6 (2020) 2000648.
[12] T. Zhang, Y. Liu, B. Hu, et al., Chin. Chem. Lett. 30 (2019) 949–952.
[13] Z.Z. Ma, Z.F. Shi, L.T. Wang, et al., Nanoscale 12 (2020) 3637–3645.
[14] L. Su, X. Zhang, Y. Zhang, A.L. Rogach, Top. Curr. Chem. 374 (2016) 42.
[15] Z. Wang, B. Chen, A.S. Susha, et al., Adv. Sci. 3 (2016) 1600182.
[16] Z. Wang, A.S. Susha, B. Chen, et al., Nanoscale 8 (2016) 7197–7202.
[17] P.S. Kuttipillai, Y. Zhao, C.J. Traverse, et al., Adv. Mater. 28 (2016) 320–326.
[18] Z. Yin, Z. Wang, X. Dai, et al., ACS Sustain. Chem. Eng. 8 (2020) 15336–15343.

[19] A. Aires, V. Fernandez-Luna, J. Fernandez-Cestau, R.D. Costa, A.L. Cortajarena, Nano Lett. 20 (2020) 2710–2716.
[20] P. Sun, Z. Wang, Y. Bi, et al., ACS Appl. Nano Mater. 3 (2020) 2038–2046.
[21] H.H. Deng, Q.Q. Zhuang, K.Y. Huang, et al., Nanoscale 12 (2020) 15791–15799.
[22] Z. Lionet, T.H. Kim, Y. Horiuchi, S.W. Lee, M. Matsuoka, J. Phys. Chem. C 123 (2019) 27501–27508.
[23] Y. Liu, P. Gao, C. Huang, Y. Li, Sci. China Chem. 58 (2015) 1553–1560.
[24] Y. Nakabayashi, Y. Nosaka, Phys. Chem. Chem. Phys. 17 (2015) 30570–30576.
[25] Y. Wu, Y. Gao, J. Du, Talanta 197 (2019) 599–604.
[26] Y. Jiang, Y. Zhu, Y. Zheng, et al., Food Chem. 338 (2021) 128158.
[27] K.C. Duong-Ly, S.B. Gabelli, Methods Enzymol. 541 (2014) 85–94.
[28] A. Baksi, P.L. Xavier, K. Chaudhari, et al., Nanoscale 5 (2013) 2009–2016.
[29] Z. Wu, J. Liu, Y. Gao, et al., J. Am. Chem. Soc. 137 (2015) 12906–12913.
[30] H.Y. Huang, K.B. Cai, M.J. Talite, et al., Sci. Rep. 9 (2019) 4053.
[31] T.D. Bennett, A.K. Cheetham, Acc. Chem. Res. 47 (2014) 1555–1562.
[32] P. Sun, Z. Wang, D. Sun, et al., J. Colloid Interface Sci. 567 (2020) 235–242.
[33] Z. Zhao, D. Yang, H. Ren, et al., Chem. Eng. J. 400 (2020) 125929.
[34] M. Mohammad, M. Lisiecki, K. Liang, A. Razmjou, V. Chen, Appl. Mater. Today 21 (2020) 100884.